

Chapter 1

Introduction

1.1 Introduction

In the beginning of the present century the discovery of the first quantum effects associated with the radiation of light from atoms, presented a serious riddle to the established community of physics. It was until then a commonly accepted fact that physics developed so far was capable of explaining *all* the phenomena of nature if one was just sufficiently detailed and patient. It was therefore natural to expect that the new quantum phenomena could be suitably explained just by hard work. By the success of the Bohr postulates and the calculation of the Rydberg constant and the energy levels of the hydrogen atom, it became clear that at least some minor modifications were needed to explain the physics going on on the atomic scale. It was first noted by Einstein [26] that the methods developed by Bohr and Sommerfeld would not be capable of describing generic systems that display chaos. Later by the failure of the Bohr-Sommerfeld model in describing the energy levels of Helium, it indeed turned out that it was necessary to introduce some drastical new concepts. This realization led in the following years to the development of the theory of quantum mechanics as we know it today.

With the development of chaos theory a new interest in the old quantum theory arose. It has been realized that dynamical systems in general display a very complicated and unpredictable behavior - *chaos*, which means that the integrable case which provided the first success of the Bohr-Sommerfeld model is rather an exception than a rule. With the work of Gutzwiller [35] the importance of classical orbits in quantum systems which has a chaotic underlying classical dynamics became evident. The Gutzwiller trace formula expresses the density of states of a quantum system as a sum over the periodic orbits of the corresponding classical system. Various resummation techniques can be applied to the Gutzwiller trace formula, yielding altogether one of the principal bodies of theoretical methods available for the analysis of quantum systems whose classical analogs are chaotic. Considerable progress has been made along these lines in the recent years, and new methods have appeared for understanding

a variety of systems in atomic, molecular and nuclear physics. Many of these results are in a sense just improvements of the Gutzwiller trace formula, having different advantages as for instance in their convergence properties. It is along this line of work the present thesis should be considered a small contribution. In the following sections we shall try to describe our search for improvements and variations on the theme of Gutzwiller.

A guide to the busy reader

The content of the following thesis might, at a first sight, seem quite overwhelming. However, because the work follows mainly three different directions, a lot of different basic material, which should not be considered as a main part of the original work, has been included. To help the reader to focus on the part of the thesis I find is due to my own work it is therefore appropriate here to sketch an outline of the following sections:

1. In section **2**, we introduce the 3-disk scattering system and describe the properties of this in order to be able to use this as an example for numerical studies throughout the following sections. This section should not provide any dramatic new information since it is based on work by Gaspard and Rice[32], and on several articles by Cvitanović [12].
2. In section **3,4**, we describe the results on flows, semiclassical quantization and cycle expansions obtained in the recent years before the start of the present work. This work should also be well known for people within the field of classical chaos and semiclassical quantization, and is only included for self consistency of the thesis.
3. The last three sections however, should finally contain my own contributions, but of course also here I have to relay on results recently obtained by others. In section **5**, we start by studying the first attempt (the quantum Fredholm determinant) to improve the convergence properties of semiclassical spectral determinants. This work is based on the articles of Cvitanović and Rosenqvist [13] and on the article by Cvitanovic, Rosenqvist, Rugh and Vattay [14]. Next we investigate the evolution operator introduced by G. Vattay [53], which has the property that it is multiplicative and therefore results in an entire spectral determinant. My work here consists in obtaining the general expression for this in the N -dimensional case, and exemplify the results with a few numerical examples.
4. In section **6**, we first describe the theory of geometrical optics by Keller [38, 39], and then use his results and the work by Franz [28] to introduce new generalized diffractive periodic orbits in the Gutzwiller trace formula. This work was done together with G. Vattay and A. Wirzba and resulted in the articles [54].
5. Finally in section **7**, we described the recent theory of G. Vattay [55] on how to calculate \hbar corrections to the Gutzwiller trace formula (or the re-

lated Gutzwiller-Voros zeta function), by studying local Schrödinger problems in the neighbourhood of the classical periodic orbits of the system. It should be emphasized that we take this theory as a starting point for the further work in the section and that we do not want to steal the credit for the original idea which is solely due to G. Vattay. My contribution in this section is therefore to specialize the theory to 2-dimensional billiard systems, to develop a simple numerical code (listed in the appendix) that calculates the first \hbar correction for any 2-dimensional billiard system and finally to use this code for numerical studies on the 3-disk system.

6. To minimize the content of the main part of the thesis I have decided to postpone a lot of the tedious derivations to a couple of appendices. These derivations can be interesting if one would like to go through all the detailed calculations but I think that in general they would lower the readability of the main part of the work which is already bothered with a lot of tedious calculations. In the main text I have indicated which derivations one can find (at least a sketch of) in these appendices. As mentioned above we also list the FORTRAN code which has been used for calculating the \hbar corrections in the 3-disk scattering system.

It is my hope that the above considerations should provide readers, who are already familiar with these topics, with a useful guide to find their way through the thesis.

Chapter 2

The laboratory

2.1 Classical Pinball

The model that we shall use for numerical studies throughout this thesis is simple, yet physical and instructive. One can use it to illustrate almost everything one needs to know about deterministic chaos: from Smale horseshoes, Cantor sets, Lyapunov exponents, symbolic dynamics, discrete symmetries, bifurcations, pruning and diffusion, all the way to transfer operators, thermodynamic formalism, and classical and quantum zeta functions.

Our classical pinball model consists of a point particle and three identical circular disks in the plane (fig. 2.1a).

The point particle is scattered elastically off the disks and moves freely between collisions. The dynamics with one or two disks is simple (there is either no or one trapped trajectory), but with three or more disks there are infinitely many trapped trajectories, forming a repeller. This repeller can be in principle observed by measurements such as irregularly fluctuating outgoing angles *vs.* impact parameter (the irregular or chaotic scattering[23]), but such measurements are difficult and very sensitive to small perturbations. Much more robust are the global averages of quantities such as the mean trapping time in the classical case or the scattering resonances in the quantum mechanical case.

2.2 Symmetries of the model

As the three disks are equidistantly spaced, the system has the C_{3v} symmetry. Applying an element (identity, rotation by $\pm 2\pi/3$, or reflection) of this symmetry group to any trajectory yields another dynamically acceptable trajectory. Symmetry operations map *nonsymmetric* orbits into different orbits of the same shape, and for a *symmetric* orbit, the symmetry operation will map the set of points making up the orbit in phase space into itself.

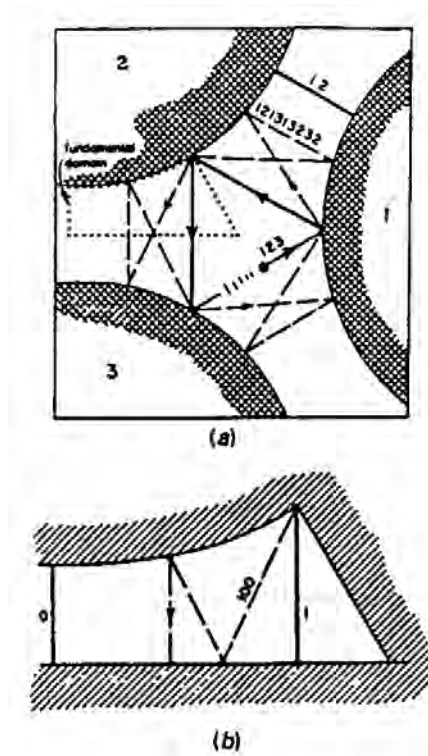


Figure 2.1: The scattering geometry for the disk radius/separation ratio $a : R = 1 : 2.5$. (a) the three disks, with $\overline{12}$, $\overline{123}$ and $\overline{121313232}$ cycles indicated. (b) the fundamental domain, *ie.* a wedge consisting of a section of a disk, two segments of symmetry axes acting as straight mirror walls, and an escape gap. The above cycles restricted to the fundamental domain are now the two fix points $\overline{0}$ and $\overline{1}$ and the $\overline{100}$ cycle.

For symmetric periodic orbits (a trajectory is periodic if it returns to the starting position and momentum in phase space) some or all symmetry operations act like a shift in time, advancing the starting point to the starting point of a symmetry related segment. In this way a symmetric periodic trajectory can be subdivided into a sequence of irreducible segments. Stability, action and traversal time is the same for all irreducible segments. The global periodic orbits can be described completely in terms of the irreducible segments, by folding the irreducible segments into periodic orbits in the *fundamental domain* [16]. The fundamental domain is a one sixth slice of the full 3-disk system, with the symmetry axes acting as reflecting mirrors, see fig. 2.1b.

Orbits related in the full space by discrete symmetries map onto a single fundamental domain orbit. The reduction to the fundamental domain desymmetrizes the dynamics and removes all global discrete symmetry induced degeneracies: rotationally symmetric global orbits have degeneracy 2, reflectionally symmetric ones have degeneracy 3, and global orbits with no symmetry are 6-fold degenerate. The time-reversal degeneracies persist in the fundamental domain as well. Some examples of such orbits are shown in fig. 2.2.

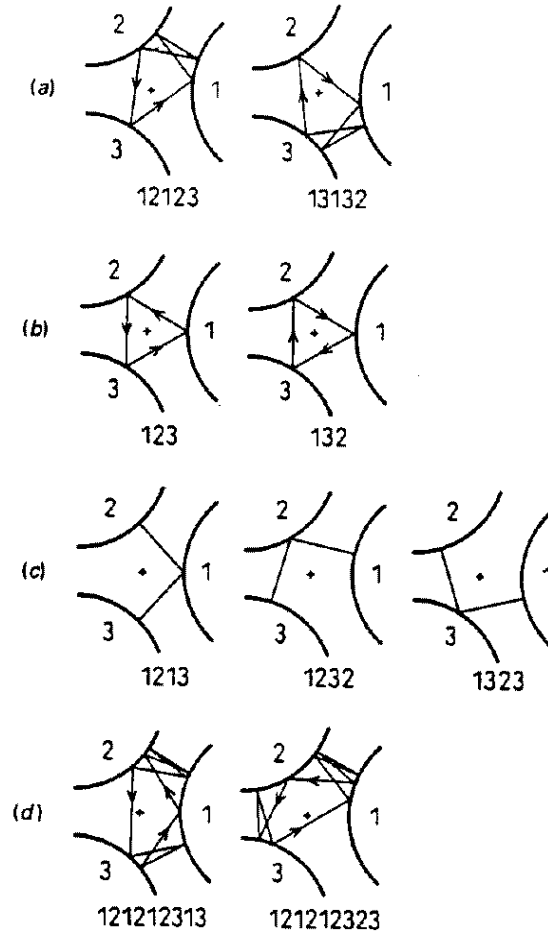


Figure 2.2: Some examples of 3-disk cycles. (a) $\overline{12123}$ and $\overline{13132}$ are mapped into each other by σ_{23} , the flip across 1 axis; this orbit has degeneracy 6 under C_{3v} symmetries. Similarly (b) $\overline{123}$ and $\overline{132}$ and (c) $\overline{1213}$, $\overline{1232}$ and $\overline{1323}$ are degenerate under C_{3v} . The orbits (d) $\overline{121212313}$ and $\overline{121212323}$ are related by time reversal but not by any C_{3v} symmetry.

2.3 Symbolic coding

The motion of a point particle is such that after a collision with one disk it either continues to another disk or it escapes to infinity. Labelling the disks 1, 2 and 3, this suggests associating with every trajectory a sequence of labels, indicating the disks with which the particle collides. The collision sequence will be finite for a scattering orbit, coming in from infinity and escaping after a finite number of collisions, and it will repeat periodically for a (trapped) periodic orbit. Arguments used in the usual horseshoe construction show that among the infinitely long sequences and the infinitely long unstable trapped orbits there is a one-to-one relationship; there exists an orbit to every (allowed) infinite sequence and every (allowed) infinite sequence labels a unique orbit.

There is one obvious restriction to the possible sequences, namely that two consecutive symbols must not be identical, since the particle cannot collide two times in succession with the same disk. In addition, there are relabeling symmetries, relating for instance the periodic orbits $\overline{12}$, $\overline{23}$, and $\overline{13}$, which are mapped into the same fundamental domain orbit. (A bar over a sequence indicates periodic repetitions; it will often be omitted when it is clear from the context that we are dealing with periodic orbits). By replacing the absolute disk labels by relative symbols, indicating only the orientation of the motion (clockwise or anticlockwise), both the symbol repetitions and the symmetry degeneracy are removed. We shall use the symbol 1 to indicate that the orientation after collision is kept, and the symbol 0 to indicate that it is reversed. Depending on the symmetry of the global orbit, periodically continued binary string labels correspond either to the full periodic orbit or to a repeating irreducible segment (examples are shown in fig. 2.1). If the disks are sufficiently far apart¹ there are no further restrictions on symbols, and all periodic binary sequences are realized as allowed periodic orbits. Table 2.1 lists some of the shortest binary symbol strings, together with the corresponding full 3-disk symbol sequences and orbit symmetries.

2.4 Counting prime cycles

In order to use the cycles of the system in our semiclassical determinants it is essential that we get all of the orbits up to a certain length. It is therefore necessary to be able to count the orbits in order not to miss any of them. For the ternary dynamics the number of periodic orbits of length n is simply $N_n^{(3)} = 3 \cdot 2^{n-1}$, since we are not allowed any consecutive bounce on the same disk. For the binary symbolic dynamics we get $N_n^{(2)} = 2^n$ since we have no pruning. Having calculated the number of periodic points, our next objective is to evaluate the number of prime cycles M_n for a dynamical system whose symbolic dynamics is built from N symbols. The problem of finding M_n is

¹For ratios $R : a \geq 2.04821419 \dots$ there is no pruning of the system [49], and thus all the possible symbol sequences correspond to physically realizable periodic orbits.

\tilde{p}	p	$\mathfrak{S}_{\tilde{p}}$
0	1 2	σ_{12}
1	1 2 3	C_3
01	12 13	σ_{23}
001	121 232 313	C_3
011	121 323	σ_{13}
0001	1212 1313	σ_{23}
0011	1212 3131 2323	C_3^2
0111	1213 2123	σ_{12}
00001	12121 23232 31313	C_3
00011	12121 32323	σ_{13}
00101	12123 21213	σ_{12}
00111	12123	e
01011	12131 23212 31323	C_3
01111	12132 13123	σ_{23}
000001	121212 131313	σ_{23}
000011	121212 313131 232323	C_3^2
000101	121213	e
000111	121213 212123	σ_{12}
001011	121232 131323	σ_{23}
001101	121231 323213	σ_{13}
001111	121231 232312 313123	C_3
010111	121312 313231 232123	C_3^2
011111	121321 323123	σ_{13}

Table 2.1: C_{3v} correspondence between the binary labeled fundamental domain prime cycles \tilde{p} and the full 3-disk ternary $\{1,2,3\}$ cycles p , together with the C_{3v} transformation that maps the end point of the \tilde{p} cycle into the irreducible segment of the p cycle. The degeneracy of p cycle is $m_p = 6n_{\tilde{p}}/n_p$.

classical in combinatorics (counting necklaces made out of n beads out of N different kinds) and is easily solved. There are N^n possible distinct strings of length n composed of N letters. These N^n strings include all M_d prime d -cycles whose period d equals or divides n . A prime cycle is a non-repeating symbol string: for example, $p = \overline{011} = \overline{101} = \overline{110} = \dots 011011\dots$ is prime, but $\overline{0101} = \overline{010101\dots} = \overline{01}$ is not. A prime d -cycle contributes d strings to the sum of all possible strings, one for each cyclic permutation. The total number of possible periodic symbol sequences of length n is therefore related to the number of prime cycles by

$$N_n = \sum_{d|n} dM_d, \quad (2.1)$$

where N_n equals $\text{tr}T^n$. The number of prime cycles can be computed recursively

$$M_n = \frac{1}{n} \left(N_n - \sum_{d|n, d < n} dM_d \right),$$

or by the *Möbius inversion formula*

$$M_n = n^{-1} \sum_{d|n} \mu \left(\frac{n}{d} \right) N_d. \quad (2.2)$$

where the Möbius function $\mu(1) = 1$, $\mu(n) = 0$ if n has a squared factor, and $\mu(p_1 p_2 \dots p_k) = (-1)^k$ if all prime factors are different.

2.5 Periodic orbits

There is only one length scale in the system, the ratio of the center-to-center separation to the disk radius $R : a$. The energy is a quadratic function of momenta, $H = p^2/2m$, so motion at different energies E and E_0 is related by the scaling $p_E \rightarrow p_0 \sqrt{E/E_0}$ for momenta, $t_E \rightarrow t_0 \sqrt{E_0/E}$ for times, and

$$S(E) = L\sqrt{2mE} = S(E_0)\sqrt{E/E_0} \quad (2.3)$$

for the actions, where L is the geometrical length of the orbit. The eigenvalues of the Jacobian transverse to a periodic orbit (see below) are invariant under the above energy rescaling. These observations will be useful below in the semiclassical context where (2.3) will combine with \hbar to the relevant quantum variable, the wavenumber $k = \sqrt{2mE}/\hbar$.

The motion between collisions is completely characterized by an angle φ marking the point of collision along a disk and the impact parameter $b = \tilde{b}/R$ measured in units of the radius. Because of symmetry, we can always select the disk 1 as the disk of current collision and the disk 3 as the origin of the particle. Ingoing coordinates then are (φ_{in}, b_{in}) and outgoing coordinates are $(\tilde{\varphi}_{out}, \tilde{b}_{out})$, where the $\tilde{}$ indicates that these coordinates refer to the next collision disk. When working in the fundamental domain they still need to be mapped back onto disk 2. Accordingly, we have two types of collisions:

- 0: the particle returns to the disk it is coming from
- 1: the particle continues to the next disk.

The corresponding maps are (the angle φ is measured clockwise relative to the line connecting the centers of disks 1 and 3)

$$T_0 : \begin{cases} \varphi_{out} = -\varphi_{in} + 2 \arcsin b_{in} \\ b_{out} = -b_{in} + \frac{d}{R} \sin \varphi_{out} \end{cases} \quad (2.4)$$

for reflection and

$$T_1 : \begin{cases} \varphi_{out} = \varphi_{in} - 2 \arcsin b_{in} + \varphi_{shift} \\ b_{out} = b_{in} - \frac{d}{R} \sin \varphi_{out} \end{cases} \quad (2.5)$$

with $\varphi_{shift} = 2\pi/3$ for the case of continuation. Each map has a fixed point, corresponding to the orbits $\bar{0}$ and $\bar{1}$. Longer periodic orbits are fixed points of sequences of maps, e.g.

$$T_0 T_0 T_1 T_0 T_1 x_{10100} = x_{10100} , \quad (2.6)$$

(note that in our convention the maps are applied in reverse order compared to the symbolic sequence).

The Jacobian of the single collision map is given by

$$J_i = \frac{\partial T_i(\varphi_{in}, b_{in})}{\partial(\varphi_{in}, b_{in})} \quad (2.7)$$

and the cycle Jacobian J_p is given by the product of Jacobians for the bounces around the cycle p . As the dynamics is phase-space volume preserving, $\det J = 1$ and the eigenvalues depend only on $tr(J)$:

$$\Lambda_{\pm} = \frac{1}{2} \left(tr(J) \pm \sqrt{tr(J)^2 - 4} \right) . \quad (2.8)$$

The sign of the eigenvalue depends of the number of collisions along the cycle. For the '0' symbol there are two bounces in the fundamental domain: one with the disk and one with the reflecting wall. Since the wall can be regarded as a disk of infinite radius, the trace changes sign two times and thus the eigenvalues are positive. Symbol '1' corresponds to one bounce with the disk but two wall bounces and hence the eigenvalues of the '1'-cycle are negative. For an arbitrary fundamental domain cycle, the eigenvalue sign is given by $(-1)^{n_1}$, where n_1 is the number of '1's in the binary string corresponding to the cycle.

The exact lengths and eigenvalues of $\bar{0}$, $\bar{1}$ and $\bar{10}$ cycles follow from elementary geometrical considerations (we set the disk radius $R = 1$ throughout). For the fundamental domain $\bar{0}$ (the 2-cycle of the complete 3-disk space) and $\bar{1}$ (the 3-cycle of the complete 3-disk space) fixed points we obtain

$$\begin{aligned} \bar{0}: \quad L_0 &= d - 2 & \Lambda_0 &= (d - 1) + \sqrt{(d - 1)^2 - 1} \\ \bar{1}: \quad L_1 &= d - \sqrt{3} & \Lambda_1 &= -\left(\frac{2}{\sqrt{3}}d - 1\right) - \sqrt{\left(\frac{2}{\sqrt{3}}d - 1\right)^2 - 1} \end{aligned} , \quad (2.9)$$

and for the $\bar{10}$ -cycle we obtain

$$\bar{10}: \quad L_{10} = \sqrt{1 + (2d - \sqrt{3})^2} - 2, \quad tr(J_{10}) = \frac{L_{10}(L_{10}+1)(L_{10}+2)}{\sqrt{3}d/2-1} + 2L_{10} + 2 .$$

Λ_{10} then follows from (2.8). Longer cycles require numerical evaluation by methods such as orbit length minimization, which we describe in section (2.7). Formulas for evaluation of the cycle Jacobians we are going to study in the following section.

2.6 Cycle stability for billiards

Consider a 2-dimensional billiard with phase space coordinates (q_1, q_2, p_1, p_2) . Let t_k be the instant of the k -th collision of the billiard with the billiard boundary, and $t_k^\pm = t_k \pm \epsilon$, ϵ positive and infinitesimal. Setting the mass and the velocity equal to 1, we impose the energy conservation by parametrizing the momentum direction by angle θ , $(q_1, q_2, \sin \theta, \cos \theta)$. Now parametrize the 2- d neighborhood of a trajectory segment between $(k-1)$ -th and k -th collisions by $\delta x = (\delta\theta, \delta z)$, where δz_k is the coordinate variation transverse to the k -th segment of the flow. Using $dq_i/dt = p_i$, we obtain the equations of motion for the linearized neighborhood

$$\frac{d}{dt}\delta\theta = 0, \quad \frac{d}{dt}\delta z = \delta\theta.$$

Let $\delta\theta_k = \delta\theta(t_k^+)$ and $\delta z_k = \delta z(t_k^+)$ be the local coordinates immediately after the k -th collision, and $\delta\theta_k^- = \delta\theta(t_k^-)$, $\delta z_k^- = \delta z(t_k^-)$ immediately before. Integrating the free flight from t_{k-1}^+ to t_k^- we obtain

$$\begin{aligned} \delta\theta_k^- &= \delta\theta_{k-1} \\ \delta z_k^- &= \delta z_{k-1} + \tau_k \delta\theta_{k-1}, \quad \tau_k = t_k - t_{k-1}, \end{aligned} \quad (2.10)$$

and the transverse Jacobian is given by

$$\mathbf{J}_T(x_k) = \begin{bmatrix} 1 & 0 \\ \tau_k & 1 \end{bmatrix}.$$

At incidence angle ϕ_k (the angle between the outgoing particle and the outgoing normal to the billiard edge), the incoming transverse variation δz_k^- projects onto an arc on the billiard boundary of length $\delta z_k^- / \cos \phi_k$. The corresponding incidence angle variation $\delta\phi_k = \delta z_k^- / R_k \cos \phi_k$, $R_k =$ local radius of curvature, increases the angular spread to

$$\begin{aligned} \delta\theta_k &= -\delta\theta_k^- - \frac{2}{R_k \cos \phi_k} \delta z_k^- \\ \delta z_k &= -\delta z_k^-, \end{aligned} \quad (2.11)$$

so the Jacobian associated with the reflection is

$$\mathbf{J}_R(x_k) = - \begin{bmatrix} 1 & r_k \\ 0 & 1 \end{bmatrix}, \quad r_k = \frac{2}{R_k \cos \phi_k}.$$

The Jacobian of a cycle p of length n_p is therefore given by

$$\mathbf{J}_p = (-1)^{n_p} \prod_{k=1}^{n_p} \begin{bmatrix} 1 & r_k \\ 0 & 1 \end{bmatrix} \begin{bmatrix} 1 & 0 \\ \tau_k & 1 \end{bmatrix}. \quad (2.12)$$

As $\det \mathbf{J} = 1$, the sign of the leading eigenvalue depends only on the trace of the determinant: $\Lambda = \frac{1}{2}(\text{Tr} J \pm \sqrt{\text{Tr}^2 J - 4})$, and by (2.12) the trace after n compositions of the determinants has the sign $(-1)^n$, *ie.* the eigenvalues flip sign at each collision. This yields a convenient way of finding the correct sign of the stabilities in the fundamental domain, since a straight wall can be considered as the limit of a disk whose radius tends to infinity. A typical set of the periodic orbit data, for $d : R = 6$ and length ≤ 6 , is listed in 2.2.

period	Λ_p	Action	code
1	9.898979485566E+00	4.000000000000	0
1	-1.177145519638E+01	4.267949192431	1
2	-1.240948019921E+02	8.316529485168	01
3	-1.240542557041E+03	12.321746616182	001
3	1.449545074956E+03	12.580807741032	011
4	-1.229570686196E+04	16.322276474382	0001
4	1.445997591902E+04	16.585242906081	0011
4	-1.707901900894E+04	16.849071859224	0111
5	-1.217338387051E+05	20.322330025739	00001
5	1.432820951544E+05	20.585689671758	00011
5	1.539257907420E+05	20.638238386018	00101
5	-1.704107155425E+05	20.853571517227	00111
5	-1.799019479426E+05	20.897369388186	01011
5	2.010247347433E+05	21.116994322373	01111
6	-1.205062923819E+06	24.322335435738	000001
6	1.418521622814E+06	24.585734788507	000011
6	1.525597448217E+06	24.638760250323	000101
6	-1.688624934257E+06	24.854025100071	000111
6	-1.796354939785E+06	24.902167001066	001011
6	-1.796354939785E+06	24.902167001066	001101
6	2.005733106218E+06	25.121488488111	001111
6	2.119615015369E+06	25.165628236279	010111
6	-2.366378254801E+06	25.384945785676	011111

Table 2.2: Classical periodic orbits for the three disk system at $d : R = 6$. The columns list the symbolic period, the instability Λ_p , the length or action of the orbit and the binary symbolic coding of the orbit. Note the two period 6 orbits $\overline{001011}$ and $\overline{001101}$, which have the same action and stability; they are related by time reversal symmetry but not by any discrete spatial symmetry.

2.7 Orbit length minimization method

The simplest method for determining billiard cycles is given by the principle of least action, or, equivalently, by minimizing the length of an approximate orbit that visits a given sequence of disks. In contrast to the multipoint shooting method which requires variation of $2N$ phase-space points, minimization of the cycle length requires variation of only N bounce positions s_i , $i = 1, 2, \dots, N$. In the following we shall see that this variation indeed can be accomplished by considering only a one-dimensional minimization problem.

The method works for any billiard system but let us for now assume that we are working with N non-intersecting disks with radii R_i . Let the point (x_i, y_i) denote the center of the i 'th disk, and $s_i^{(0)}$ be the initial guess of the i 'th bouncing position, which is an angle measured with respect to some fixed point on the surface of the i 'th disk. The length (or equivalently, the period or the action) of the initial approximate cycle is given by

$$L^{(0)} = \sum_{i=1}^N l_i^{(0)} = \sum_{i=1}^N [(\Delta x_i^{(0)})^2 + (\Delta y_i^{(0)})^2]^{1/2}$$

where $\Delta x_i^{(0)} \equiv x_{i+1} - x_i + R_{i+1} \cos(s_{i+1}^{(0)}) - R_i \cos(s_i^{(0)})$, $x_{N+1} \equiv x_1$, and similarly for $\Delta y_i^{(0)}$. The idea is now the following: taking the gradient of $L^{(0)}$ gives us the direction in \mathbf{s} space in which the total length decreases with the highest rate. Following this direction until we reach a minimum defines a new point $\mathbf{s}^{(1)}$ which is now the next approximation to the real cycle. Iterating this procedure then finally leads to a cycle that obeys the Fermat principle and therefore is the cycle we are interested in. In our case the gradient of the length function in the j 'th approximation can be obtained directly and reads:

$$\begin{aligned} (\vec{\nabla} L^{(j)})_i &= \frac{\partial l_{i-1}^{(j)}}{\partial s_i^{(j)}} + \frac{\partial l_i^{(j)}}{\partial s_i^{(j)}} \\ &= R_i \left(\sin(s_i^{(j)}) \left(\frac{\Delta x_i^{(j)}}{l_i^{(j)}} - \frac{\Delta x_{i-1}^{(j)}}{l_{i-1}^{(j)}} \right) - \cos(s_i^{(j)}) \left(\frac{\Delta y_i^{(j)}}{l_i^{(j)}} - \frac{\Delta y_{i-1}^{(j)}}{l_{i-1}^{(j)}} \right) \right). \end{aligned}$$

The minimization algorithm can now be implemented by following the recursion scheme:

1. Select an initial set of bounce positions \vec{s}_0 .
2. Evaluate $\vec{\nabla} L |_{\vec{s}=\vec{s}_0}$.
3. Minimize L along the hyper line spanned by the above gradient, *ie.* minimize the function $L(\vec{s}_0 + \vec{\nabla} L |_{\vec{s}=\vec{s}_0} \cdot t)$ with respect to the parameter t .
4. Use the bounce points \vec{s}_1 so determined as the starting point for the next iteration of the algorithm, and proceed iterating items 2,3 and 4 until the desired accuracy is attained.

5. If the dynamics is pruned, check that the final minimal length orbit does not penetrate any of the disks.

One way to ensure that the algorithm has obtained the limit of the procedure is to evaluate the gradient (or the length of the gradient) at the different points $\mathbf{s}^{(0)}, \mathbf{s}^{(1)}, \mathbf{s}^{(2)}, \dots$. In practice when the length of the gradient is zero up to accuracy of the implemented precision (quadruple precision $0 \simeq 10^{-32}$), further iteration does not alter the bouncing positions. It turns out that the algorithm converges very fast to this limit, of course depending on the initial guess and the length of the cycle. To get a good initial guess, one can construct the following $\mathbf{s}^{(0)}$: first you consider the full space itinerary $\alpha_1, \alpha_2, \dots, \alpha_{n_p}$ that describes the sequence in which the disks are visited by the cycle. To construct $s_i^{(0)}$ we then consider the two line segments that connects the centers of the previous and following disk to the center of the current disk. Then $s_i^{(0)}$ can be set as the angle that divides the angle spanned by these two line segments in two equal parts.

The above method has been applied succesfully to the 3-disk system at three different disk-disk separations, namely with $R : a = 3$, $R : a = 6$ and $R : a = 12$, and all orbits up to topological length (in binary alphabet) 12 have been obtained. Besides this we have also [44] checked the method on the 7- and 13-disk systems where the disks have been positioned as first and second approximations to the Lorentz gas [44].

Chapter 3

Classical periodic orbit theory

3.1 Flows, evolution operators and their spectra

Functional determinants and zeta functions arise in classical and quantum mechanics because in both the dynamical evolution can be described by the action of linear evolution operators on infinite-dimensional vector spaces. The classical *evolution operator* for a d -dimensional map or a $(d + 1)$ -dimensional flow is given by:

$$\mathcal{L}^t(y, x) = \delta(y - f^t(x))g^t(x) . \quad (3.1)$$

For discrete time, $f^n(x)$ is n -th iterate of the map f ; for continuous flows, $f^t(x)$ is the trajectory of the initial point x . $g^t(x)$ is a weight multiplicative along the trajectory; its precise functional form depends on the dynamical average under study. For purposes of this section it suffices to take $g^t(x) = 1$, essentially the Perron-Frobenius operator case.

The global averages (escape rates, energy eigenvalues, resonances, fractal dimensions, etc.) can be extracted from the eigenvalues of the evolution operators. The eigenvalues are given by the zeros of appropriate determinants. One way to evaluate determinants is to expand them in terms of traces, $\log \det = \text{tr} \log$, and in this way relate the spectrum of an evolution operator to its traces, *ie.* the periodic orbits of the system. Formally, the traces $\text{tr} \mathcal{L}^t$ are easily evaluated as integrals of Dirac delta functions as follows.

3.1.1 Trace formula for maps

If the evolution is given by a discrete time mapping, and all periodic points are known to have stability eigenvalues $\Lambda_k \neq 1$ strictly bounded away from unity,

the trace \mathcal{L}^n is given by the sum over all periodic points x of period n :

$$\begin{aligned} \text{tr}\mathcal{L}^n &= \int dx dy \delta(x-y) \mathcal{L}^n(y, x) \\ &= \sum_p n_p \sum_{r=1}^{\infty} \frac{\delta_{n, n_p r}}{|\det(\mathbf{1} - \mathbf{J}_p^r)|}, \end{aligned} \quad (3.2)$$

where

$$\mathbf{J}_p(x) = \prod_{j=0}^{n_p-1} \mathbf{J}(f^j(x)), \quad J_{kl}(x) = \frac{\partial}{\partial x_l} f_k(x) \quad (3.3)$$

is the $[d \times d]$ Jacobian matrix evaluated at the periodic point x , and the product goes over all periodic points x_i belonging to a given prime cycle p . The *trace formula* is the Laplace transform of $\text{tr}\mathcal{L}^t$ which, for discrete flows, is simply the generating function

$$\text{tr}\mathcal{L}(z) = \sum_{n=1}^{\infty} z^n \text{tr}\mathcal{L}^n = \sum_{\alpha=0}^{\infty} \frac{z e^{-\nu_\alpha}}{1 - z e^{-\nu_\alpha}}$$

where $e^{-\nu_0}, e^{-\nu_1}, e^{-\nu_2}, \dots$ are the eigenvalues of \mathcal{L} . For large times $\det(\mathbf{1} - \mathbf{J}^{(n)}(x_i)) \rightarrow \Lambda_i$, where Λ_i is the product of the expanding eigenvalues of $\mathbf{J}^{(n)}(x_i)$, so the trace is dominated by

$$\begin{aligned} \text{tr}\mathcal{L}(z) &\approx \sum_{n=1}^{\infty} z^n \sum_{x_i \in \text{Fix}(f^n)} \frac{1}{|\Lambda_i|} \\ &= \frac{z e^{-\nu_0}}{1 - z e^{-\nu_0}} + \dots, \end{aligned} \quad (3.4)$$

and diverges at the leading eigenvalue $1/z = e^{-\nu_0}$. This approximation, which in current physics literature is called the “thermodynamic” or the “ f of α ” formalism [36], is adequate (but far from optimal) for extraction of the leading eigenvalue of \mathcal{L} , and difficult to apply to extraction of the non-leading eigenvalues.

3.1.2 Trace formula for flows

For flows the eigenvalue corresponding to the eigenvector along the flow (the velocity vector) necessarily equals unity for all periodic orbits, and therefore the integral (3.2) requires a more careful treatment [17].

To evaluate the contribution of a prime periodic orbit p of period T_p , one chooses a local coordinate system with a longitudinal coordinate dx_{\parallel} along the direction of the flow, and d transverse coordinates x_{\perp}

$$\text{tr}_p \mathcal{L}^t = \int_{V_p} dx_{\perp} dx_{\parallel} \delta(x_{\perp} - f_{\perp}^t(x)) \delta(x_{\parallel} - f_{\parallel}^t(x)). \quad (3.5)$$

Integration is restricted to an infinitesimally thin tube V_p enveloping the cycle p .

Let $v = |\mathbf{F}(x)|$ be the velocity along the orbit, and change the longitudinal variable to $dx_{\parallel} = vd\tau$. Whenever the time t is a multiple of the cycle period T_p , the longitudinal delta function contributes a term $1/v$, canceling the corresponding factor v from the change of variables, and the integral along the trajectory yields a factor T_p :

$$\begin{aligned} \int_{V_p} dx_{\parallel} \delta(x_{\parallel} - f_{\parallel}^t(x)) &= \sum_{r=1}^{\infty} \delta(t - rT_p) \int_p d\tau \\ &= T_p \sum_{r=1}^{\infty} \delta(t - rT_p). \end{aligned} \quad (3.6)$$

Linearization of the periodic flow in a plane perpendicular to the orbit yields the same weight as for the maps:

$$\int_{V_p} dx_{\perp} \delta(x_{\perp} - f_{\perp}^{-rT_p}(x)) = \frac{1}{|\det(\mathbf{1} - \mathbf{J}_p^r)|}, \quad (3.7)$$

where \mathbf{J}_p is the p -cycle $[d \times d]$ transverse Jacobian, and we have assumed hyperbolicity, *ie.* that all transverse eigenvalues are bounded away from unity. A geometrical interpretation of weights such as (3.7) is that after the r -th return to a surface of section, the initial tube V_p has been stretched out along the expanding eigendirections, with the overlap with the initial volume given by $1/|\det(\mathbf{1} - \mathbf{J}_p^r)|$.

Substituting (3.6-3.7) into (3.5), we obtain an expression for $\text{tr } \mathcal{L}^t$ as a sum over all prime cycles p and their repetitions

$$\text{tr } \mathcal{L}^t = \sum_p T_p \sum_{r=1}^{\infty} \frac{\delta(t - rT_p)}{|\det(\mathbf{1} - \mathbf{J}_p^r)|}.$$

A Laplace transform replaces the above sum of Dirac delta functions by the *trace formula for classical flows* [17]:

$$\text{tr } \mathcal{L}(s) = \int_0^{\infty} dt e^{st} \text{tr } \mathcal{L}^t = \sum_p T_p \sum_r^{\infty} \frac{e^{sT_p r}}{|\det(\mathbf{1} - \mathbf{J}_p^r)|}. \quad (3.8)$$

We should caution the reader that in taking the Laplace transform we have ignored a possible $t \rightarrow 0_+$ volume term, as we do not know how to regularize the delta function kernel in this limit. In the quantum (or heat kernel) case this limit gives rise to the Weyl or Thomas-Fermi mean eigenvalue spacing. A more careful treatment might assign to such volume term some interesting role in the theory of classical resonance spectra.

The semi-classical evaluation of the quantum trace is considerably more laborious, but the final result, given in sect. 4.1, is very similar in form to the above classical trace.

3.1.3 Fredholm determinants

The problem with the classical (3.4), (3.8) and the Gutzwiller trace formulas (4.21) is that they diverge precisely where one would like to use them (we return to this in sect. 5.1.2). While in the physics literature on dynamically generated strange sets this does not prevent numerical extraction of reasonable “thermodynamic” averages, in the case of the Gutzwiller trace formula this leads to the perplexing observation that crude estimates of the radius of convergence seem to put the entire physical spectrum out of reach. This problem is cured by going from trace formulas to determinants, which turn out to have larger analyticity domains. For maps, the two are related by

$$F(z) = \det(1 - z\mathcal{L}) = \exp\left(-\sum_n \frac{z^n}{n} \text{tr}\mathcal{L}^n\right)$$

For flows the classical Fredholm determinant is given by

$$F(s) = \exp\left(-\sum_p \sum_{r=1}^{\infty} \frac{1}{r} \frac{e^{sT_p r}}{|\det(\mathbf{1} - \mathbf{J}_p^r)|}\right), \quad (3.9)$$

and the classical trace formula (3.8) is the logarithmic derivative of the classical Fredholm determinant

$$\text{tr}\mathcal{L}(s) = -\frac{d}{ds} \log F(s). \quad (3.10)$$

With z set to $z = e^s$, the Fredholm determinant (3.9) applies both to maps and flows. A Fredholm determinant can be rewritten as an infinite product over periodic orbits, by noting that the r sum in (3.9) is close in form to expansion of a logarithm. We cast it into such a form by expanding the Jacobian weights in terms of stability eigenvalues. For a 3-dimensional Hamiltonian flow with one expanding eigenvalue Λ , and one contracting eigenvalue $1/\Lambda$, the weight in (3.9) may be expanded as follows:

$$\begin{aligned} \frac{1}{|\det(\mathbf{1} - \mathbf{J}_p^r)|} &= \frac{1}{|\Lambda|^r (1 - 1/\Lambda_p^r)^2} \\ &= \frac{1}{|\Lambda|^r} \sum_{k=0}^{\infty} (k+1) \Lambda_p^{-kr}. \end{aligned} \quad (3.11)$$

With this we can rewrite the Fredholm determinant exponent as

$$\sum_{r=1}^{\infty} \frac{1}{r} \frac{e^{sT_p r}}{|\det(\mathbf{1} - \mathbf{J}_p^r)|} = \sum_{k=0}^{\infty} (k+1) \log\left(1 - \frac{e^{sT_p}}{|\Lambda_p| \Lambda_p^k}\right).$$

and represent the Fredholm determinant as a Selberg-type product [17]

$$\begin{aligned} F(s) &= \prod_p \prod_{k=0}^{\infty} \left(1 - t_p / \Lambda_p^k\right)^{k+1}, \\ t_p &= \frac{e^{sT_p}}{|\Lambda_p|} z^{n_p}. \end{aligned} \quad (3.12)$$

z is a book-keeping variable that we will use to expand zeta functions and determinants, set to $z = 1$ in calculations. The first ($k = 0$) zeta function in the product is the Ruelle or dynamical zeta function [45]

$$\zeta = \prod_p (1 - t_p), \quad (3.13)$$

where in general, t_p depends on the dynamical average one wishes to evaluate. The simplest example is the weight (3.12) used in computation of escape rates and correlation spectra. (3.13) also yields the leading semi-classical *quantum* resonances, if t_p is the quantum weight (4.30) associated with the cycle p .

The above heuristic manipulations are potentially dangerous, as we are dealing with infinite-dimensional vector spaces and singular integral kernels; however, the Fredholm determinants are entire functions in any dimension, provided that [48]

1. the evolution operator is *multiplicative* along the flow,
2. the symbolic dynamics is a *finite subshift*,
3. all cycle eigenvalues are *hyperbolic* (sufficiently bounded away from 1),
4. the map (or the flow) is *real analytic*, *ie.* it has a piecewise analytic continuation to a complex extension of the phase space.

The notion of Axiom A systems is a mathematical abstraction of 2 and 3. It would take us too far to give and explain the definition of the Axiom A systems (see ref. [52]). Axiom A implies, however, the existence of a Markov partition of the phase space from which 2 and 3 follow. Properties 1 and 2 enable us to represent the evolution operator as a matrix in an appropriate basis space; properties 3 and 4 enable us to bound the size of the matrix elements and control the eigenvalues.

3.2 Cycle expansions

A *cycle expansion*[19] is a series representation of a zeta function or a Fredholm determinant, expanded as a sum over *pseudo-cycles*, products of prime cycle weights t_p , ordered by increasing cycle length and instability. The products (3.13),(4.32) are really only a shorthand notation for zeta functions and determinants - for example, the zeros of the individual factors in infinite products (3.13),(4.32) are *not* the zeros of the corresponding zeta functions and determinants, and convergence of such objects is far from obvious.

3.2.1 Curvature expansions

Curvature expansions are based on the observation[19, 3, 4] that the motion in dynamical systems with finite grammar is organized around a few *fundamental* cycles; more precisely, that the cycle expansion of the dynamical zeta function (3.13) allows a regrouping of terms into dominant *fundamental* contributions t_f and decreasing *curvature* corrections c_n :

$$1/\zeta = 1 - \sum_f t_f - \sum_n c_n. \quad (3.14)$$

The fundamental cycles t_f have no shorter approximants; they are the “building blocks” of the dynamics in the sense that all longer orbits can be approximately pieced together from them. In piecewise linear approximations to the flow, $1/\zeta$ is given by the determinant for a finite Markov transition matrix, and all c_n vanish identically. Hence the designation “curvatures”; size of c_n is an indication how far the flow is from a piecewise linearization.

A typical curvature term in (3.14) is a difference of a long cycle $\{ab\}$ and its shadowing approximation by shorter cycles $\{a\}$ and $\{b\}$:

$$t_{ab} - t_a t_b = t_{ab}(1 - t_a t_b / t_{ab})$$

The orbits that follow the same symbolic dynamics, such as $\{ab\}$ and the “pseudo orbit” $\{a\}\{b\}$, lie close to each other, have similar weights, and for longer and longer orbits the differences are expected to fall off rapidly. For systems that satisfy Axiom A requirements, such as the 3-disk repeller, curvature expansions converge very well[18]. It is crucial that the curvature expansion is grouped (and truncated) by topologically related cycles and pseudo-cycles; truncations that ignore topology, such as inclusion of all cycles with $T_p < T_{max}$, will contain un-shadowed orbits, and exhibit a mediocre convergence compared with the curvature expansions.

3.2.2 Fredholm determinant cycle expansions

While for the dynamical zeta function cycle expansions the shadowing is easy to explain, the resulting convergence is not the best achievable; as explained above, Fredholm determinants are expected to be entire, and their cycle expansions should converge faster than exponentially. The Fredholm determinant cycle expansions are somewhat more complicated than those for the dynamical zeta functions. We expand the exponential representation (3.9) of $F(s)$ as a multinomial in prime cycle weights t_p

$$\begin{aligned} F_p &= 1 - \sum_{r=1}^{\infty} \frac{1}{r} \frac{t_p^r}{|\det[\mathbf{1} - \mathbf{J}_p^r]|} + \frac{1}{2} (\dots)^2 - \dots \\ &= \sum_{r=1}^{\infty} C_{p^k} t_p^k. \end{aligned}$$

This yields the cycle expansion for $F(s)$:

$$F(s) = \sum_{k_1 k_2 k_3 \dots = 0}^{\infty} \tau_{p_1^{k_1} p_2^{k_2} p_3^{k_3} \dots}$$

$$\tau_{p_1^{k_1} p_2^{k_2} p_3^{k_3} \dots} = \prod_{i=1}^{\infty} C_{p_i^{k_i}} t_{p_i}^{k_i},$$

where the sum goes over all pseudo-cycles.

3.2.3 Numerical calculations with cycle expansions

In practice we do not do anything as complicated as the expansion of the preceding section. Consider the prototype of any of the determinants we are going to evaluate numerically

$$F(z, s) = \prod_p \prod_{l=0}^{\infty} (1 - t_{p,l}(s) z^{n_p}), \quad (3.15)$$

where $t_{p,l}$ is the weight associated with the p 'th primitive cycle, and z is the book-keeping variable keeping track of the topological length n_p of the cycles. Now the product (3.15) can be written as an exponential like in (3.9)

$$F(z, s) = \exp \left(- \sum_p \sum_{l=0}^{\infty} \sum_{r=1}^{\infty} \frac{1}{r} (t_{p,l} z^{n_p})^r \right) \quad (3.16)$$

where we expanded the logarithm in the identity $x = \exp(\ln x)$. For most of the cases we are going to encounter the above l sum can be performed analytically so that we end up with

$$F(z, s) = \exp \left(- \sum_p \sum_{r=1}^{\infty} \frac{1}{r} c_p^r z^{n_p r} \right). \quad (3.17)$$

By gathering all terms of the same power in z we then finally get

$$F(z, s) = \exp \left(- \sum_{n=1}^{\infty} \text{Tr}_n z^n \right), \quad (3.18)$$

where Tr_n is just the total contribution, which is finite, from all the cycles to the power n of z . A cycle of topological length n_p will thus contribute to the sum by the powers of $z^{n_p}, z^{2n_p}, \dots, z^{rn_p}, \dots$. Adding up the contribution from all the individual cycles to the Tr_n 's can then be performed by a single loop in a program. Next we expand each of the exponentials $\exp(-\text{Tr}_n z^n)$ in a power series in z . Finally, by multiplying these power series together we obtain the final power series expansion in z of the determinant. This should then be cut off at the maximal cycle length N

$$F_N(s, z) = \sum_{n=0}^N C_n(s) z^n \quad (3.19)$$

In the final evaluation z is set to $z = 1$, but the organization by powers of z^n is crucial to the convergence of cycle expansions.

To find the zeros of the determinant, we use the standard Newton-Raphson searching algorithm. To obtain a good starting point for this one can start by scanning the area of the complex plane under investigation. One should then search for local low values of the determinant by evaluating this on a suitable grid. Having obtained these initial guesses we apply the recursion scheme

$$s_{i+1} = s_i - F_N(s_i, 1)/F'_N(s_i, 1), \quad (3.20)$$

to search for the zeros. To obtain the derivative of the determinant we can use exactly the same routine as to determine it. From (3.18) we can directly get the derivative

$$F'_N(z, s) = \left(-\sum_{n=1}^N \text{Tr}'_n z^n\right) F_N(z, s), \quad (3.21)$$

which means that in the same loop where we sum up the Tr_n 's we should merely at the same time sum up also the derivatives of these. After this one just has to make one extra power series multiplication in order to obtain $F'_N(z, s)$. Of course, also here we in the end put $z = 1$.

3.2.4 Convergence of cycle expansions

It is fairly easy to establish that for Axiom A systems the trace formulas converge exponentially with the number of cycles included. As will be explained in sect. 5.1.2, the trace formulas are not absolutely convergent where you need them, and in addition, shadowing of longer orbits by nearby pseudo-orbits is not implemented, so we will not use trace formulas at all. However, it should be noted that for systems other than Axiom A, we do not know how to improve convergence by shadowing cancellations, or define determinants that are guaranteed to be entire, and it is still possible that for generic systems determinants do not converge any better than traces.

For dynamical zeta functions geometrical estimates [3] imply that for Axiom A systems the curvature expansion coefficients fall off exponentially, $C_k \approx \tilde{C}^k$, and the expansion sums up to a pole

$$\sum_{n=0}^{\infty} C_k z^k \simeq \sum_{n=0}^{\infty} (\tilde{C}z)^k = \frac{1}{1 - \tilde{C}z}.$$

Such poles are indeed observed numerically [4]. Convergence of dynamical zeta functions cycle expansions can be accelerated by a variety of numerical methods, but both on theoretical grounds and in practice, the preferred alternative is to use Fredholm determinants instead.

3.2.5 Symmetry factorizations

Discrete symmetries of the classical dynamics play a role with which we are familiar from quantum mechanics; as they commute with the evolution operators, they can be used to decompose them and factorize the associated determinants [16]:

$$1/\zeta^{3-disk} = \prod_{\alpha} 1/\zeta_{\alpha}^{d_{\alpha}} .$$

The product is over the d_{α} -dimensional irreducible representations α of the symmetry group, in this case C_{3v} , with two 1-dimensional representations A_1 , A_2 and a pair of 2-dimensional representations E . The factorization relates each fundamental domain orbit to the corresponding degenerate set of full space orbits as follows:

symmetry	full space		A_1	A_2	E	
rotation	:	$(1 - t_{rot}^3)^2$	=	$(1 - t_{rot})$	$(1 - t_{rot})$	$(1 + t_{rot} + t_{rot}^2)^2$
reflection	:	$(1 - t_{ref}^2)^3$	=	$(1 - t_{ref})$	$(1 + t_{ref})$	$(1 - t_{ref}^2)^2$
none	:	$(1 - t_{non})^6$	=	$(1 - t_{non})$	$(1 - t_{non})$	$(1 - t_{non})^4$

Fundamental domain cycles up to length 5 are listed in table 2.1 in section 2.3, together with the symmetry factors that map them into the corresponding global orbit irreducible segments; these determine which of the above factorizations apply to a given cycle. Substituting the shortest cycles into the zeta functions, we obtain for the completely symmetric A_1 subspace:

$$\begin{aligned} 1/\zeta_{A_1}(z) = & (1 - zt_0)(1 - zt_1)(1 - z^2t_{01})(1 - z^3t_{001})(1 - z^3t_{011}) \\ & (1 - z^4t_{0001})(1 - z^4t_{0011})(1 - z^4t_{0111})(1 - z^5t_{00001})(1 - z^5t_{00011}) \\ & (1 - z^5t_{00101})(1 - z^5t_{00111})(1 - z^5t_{01011})(1 - z^5t_{01111}) \dots \end{aligned} \quad (3.22)$$

In the example at hand, with complete symbolic dynamics and no pruning rules, the cycle expanded zeta function is obtained by expanding the infinite product as a power series in z :

$$\begin{aligned} 1/\zeta_{A_1}(z) = & 1 - zt_0 - zt_1 - z^2[(t_{01} - t_1t_0)] \\ & - z^3[(t_{001} - t_{01}t_0) - (t_{011} - t_{01}t_1)] \\ & - z^4[(t_{0001} - t_0t_{001}) + (t_{0111} - t_{011}t_1) \\ & + (t_{0011} - t_{001}t_1 - t_0t_{011} + t_0t_{01}t_1)] - \dots \end{aligned} \quad (3.23)$$

For the A_2 subspace cycles with an odd number of 0's pick up an additional minus sign:

$$\begin{aligned} 1/\zeta_{A_2}(z) = & 1 + zt_0 - zt_1 + z^2[(t_{01} - t_1t_0)] \\ & - z^3[(t_{001} + t_{01}t_0) + (t_{011} - t_{01}t_1)] \\ & + z^4[(t_{0001} - t_0t_{001}) + (t_{0111} - t_{011}t_1) \\ & + (t_{0011} - t_{001}t_1 - t_0t_{011} + t_0t_{01}t_1)] - \dots \end{aligned} \quad (3.24)$$

The E subspace cycle expansion takes a somewhat less obvious form [16]:

$$\begin{aligned}
1/\zeta_E &= (1 + zt_1 + z^2t_1^2)(1 - z^2t_0^2)(1 + zt_{100} + z^2t_{100}^2)(1 - z^2t_{10}^2) \\
&\quad (1 + zt_{1001} + z^2t_{1001}^2)(1 + zt_{10000} + z^2t_{10000}^2) \\
&\quad (1 + zt_{10101} + z^2t_{10101}^2)(1 - z^2t_{10011})^2 \dots \\
&= 1 + zt_1 + z^2(t_1^2 - t_0^2) + z^3(t_{001} - t_1t_0^2) \\
&\quad + z^4 \left[t_{0011} + (t_{001} - t_1t_0^2)t_1 - t_{01}^2 \right] \\
&\quad + z^5 \left[t_{00001} + t_{01011} - 2t_{00111} + (t_{0011} - t_{01}^2)t_1 + (t_1^2 - t_0^2)t_{100} \right] \\
&\quad + \dots \tag{3.25}
\end{aligned}$$

For orbits running on one of the symmetry lines, one has to take special care[16]. All our numerical results are obtained by determining the zeros of finite cycle length truncations of the above cycle expansions, or the corresponding ones for the Gutzwiller Voros zeta function, and related expressions for semiclassical spectral determinants which we are going to study in the following sections.